Journal of Advanced Ceramics
2013, 2(4): 325–332
DOI: 10.1007/s40145-013-0079-4

ISSN 2226-4108
CN 10-1154/TQ

Research Article

Characterization of free carbon in the as-thermolyzed Si–B–C–N ceramic from a polyorganoborosilazane precursor

Adhimoolam Bakthavachalam KOUSAALYA[a], Ravi KUMAR[a,*], Shanmugam PACKIRISAMY[b]

[a]*Materials Processing Section*, *Department of Metallurgical and Materials Engineering*, *Indian Institute of Technology Madras*, *Chennai 600036*, *Tamil Nadu*, *India*
[b]*Analytical Spectroscopy and Ceramics Group*, *PCM Entity*, *Vikram Sarabhai Space Centre*, *Thiruvananthapuram 695022*, *India*

Received: May 15, 2013; Revised: August 11, 2013; Accepted: August 20, 2013

Abstract: Polyorganoborosilazane ($(B[C_2H_4–Si(CH_3)NH]_3)_n$) was synthesized via monomer route from a single-source precursor and thermolyzed at 1300 ℃ in argon atmosphere. The as-thermolyzed Si–B–C–N ceramic was characterized using X-ray diffraction (XRD) and Raman spectroscopy. The crystallization behavior of silicon carbide in the as-thermolyzed amorphous Si–B–C–N matrix was understood by XRD studies, and the crystallite size calculated using Scherrer equation was found to increase from 2 nm to 8 nm with increase in dwelling time. Concomitantly, Raman spectroscopy was used to characterize the free carbon present in the as-thermolyzed ceramic. The peak positions, intensities and full width at half maximum (FWHM) of D and G bands in the Raman spectra were used to study and understand the structural disorder of the free carbon. The G peak shift towards 1600 cm^{-1} indicated the decrease in cluster size of the free carbon. The cluster diameter of the free carbon calculated using TK (Tuinstra and Koenl) equation was found to decrease from 6.2 nm to 5.4 nm with increase in dwelling time, indicating increase in structural disorder.

Keywords: synthesis; polyorganoborosilazane; precursor-derived ceramic; Si–B–C–N; Raman spectroscopy; free carbon

1 Introduction

Processing of ceramics through thermolysis of polymeric precursors can be dated back to the late 1950s when carbon composites and carbon fibers were produced from polyacrylonitrile [1,2]. However, the pioneering work of Verbeek and Winter [3,4] and Yajima *et al*. [5–7] on processing ceramics from polymeric precursors in the middle of 1970s made organo-silicon polymers promising candidate materials for producing Si-based binary, ternary and quaternary ceramics. Since these ceramics are obtained from polymeric precursors, it is possible to utilize the advantages of employing polymer processing routes to produce, for instance, fibers [8–11] and coatings [12–15].

* Corresponding author.
E-mail: nvrk@iitm.ac.in

It is now well established that boron incorporated non-oxide silicon boroncarbonitrides (Si–B–C–N) are observed to be stable at temperatures as high as 1800–2200 ℃ in inert atmosphere, rendering them highly attractive [16–19]. Due to their exceptional thermal stability, coupled with high resistance to both crystallization [20] and oxidation [21] at elevated temperatures, excellent electrical properties [22] and high-temperature mechanical properties [23], precursor-derived Si–B–C–N quaternary ceramics (PDCs) have received growing attention in recent decades. With such immense potential, there always exists a need for producing these materials with high yields, for which single-source materials have been preferred due to their ability to control the composition on an atomic scale and also avoid phase separation [9].

However, presence of free carbon is unavoidable in most of these as-thermolyzed ceramics. The nature of bonding in free carbon, and the amount of free carbon together determine the properties of the material. The incorporated free carbon can exist in either of the two hybridized forms: sp^2 and sp^3. The sp^2 hybridized form is carbon bonded to carbon, while the sp^3 hybridized form is carbon bonded to silicon [24]. The presence of free carbon content and the ratio of sp^2 hybridization to sp^3 hybridization play vital role in determining certain properties of the derived ceramic, such as thermal stability and high-temperature mechanical property [25], resistance to crystallization [26], electrical [27] and optical [28] properties. Activity of the free carbon significantly influences thermal stability of the material, with severe mass loss at increased carbon activity [29].

Trassl *et al*. [30] has shown the segregation of free carbon in SiCN ceramic thermolyzed from polysilazane at 1200 ℃ by the appearance of D and G bands in Raman spectra, which disappear when thermolyzed above 1600 ℃. The increase and decrease in the intensity of D and G bands indicate the ordering of free carbon at first, followed by disordering, resulting in the formation of SiC with consumption of carbon. However, Mera *et al*. [31] has shown the disordered state of free carbon in SiCN ceramic processed through thermolysis of phenyl-containing poly(silylcarbodiimides) below 1500 ℃. Thermolysis above 1700 ℃ leads to the ordering of free carbon resulting in increase in the intensity of G band. Sarkar *et al*. [32] has investigated the presence of free carbon via various techniques in SiBCN ceramic from polysilazane and concluded that there is no ordered network of carbon. Gao *et al*. [33] has shown the variation of free carbon content in SiBCN and SiCN ceramics obtained from poly(carbodiimides) as precursor. The density of defects decreases with boron content, resulting in the organization of carbon when thermolyzed at 1400 ℃ in contrast to thermolysis at 1100 ℃. The initial precursor (polysilazane and polycarbodiimides) has a determining role in the nature of bonding exhibited by free carbon in the final microstructure of the ceramic, as exemplified by Colombo *et al*. [26].

While very limited literatures are available on free carbon in Si–B–C–N processed from boron-modified polysilazane [32,33], a systematic study on the exact nature of free carbon, cluster size, their variation and their bonding characteristics at higher temperatures in Si–B–C–N ceramic is lacking to the best of our knowledge. Hence, the focus of this study is to determine the ratio of sp^2 hybridization to sp^3 hybridization in free carbon present in the as-thermolyzed Si–B–C–N ceramic, characterize the cluster size and its influence on the crystallization behavior, using Raman spectroscopy and X-ray diffraction (XRD).

2 Experimental methods

2.1 Synthesis procedure

Polyorganoborosilazane was synthesized via monomer route from a single-source precursor using standard Schlenk technique in argon (Ar) atmosphere by a two-step synthesis process [16,34]. Initially, monomers containing boron were produced by hydroboration of chlorosilane, followed by ammonolysis of monomers, resulting in condensation polymerization of the reactants and subsequent formation of polyorganoborosilazane.

84.6 g of dichloromethylvinylsilane ($(CH_2{=}CH)CH_3SiCl_2$, Alfa Aesar, USA) was dissolved in 90 ml of toluene and hydroborated at 0 ℃ under vigorous stirring for 30 min through drop-wise addition in 100 ml of 2M solution of boranedimethylsulfide ($(CH_3)_2SBH_3$) in toluene (Spectrochem, India) in argon atmosphere. The stirring was continued for 16 h at room temperature (25 ℃), and subsequent evaporation of the solvent was observed along with the evaporation of the byproduct (dimethylsulfide (SMe_2)) at 60 ℃

under reduced pressure. The reaction yielded 95 g of the monomer, namely, tris(dichloromethylsilylethyl) borane ($B[C_2H_4Si(CH_3)Cl_2]_3$) in the form of a colorless, oily liquid.

The ammonolysis of the monomer was carried out subsequently for 30 min by drop-wise addition of 15 ml of ammonia to a mixture containing 60 g of monomer dissolved in 90 ml of tetrahydrofuran. The temperature was slowly increased to the boiling point of the monomer (80 ℃) under vigorous stirring. The precipitated ammonium chloride (NH_4Cl) was filtered using Whatman glass micro-fiber filter paper and the filtrate was heated at 80 ℃ under reduced pressure. This yielded 58 g of white solid lumps of polyorganoborosilazane ($(B[C_2H_4–Si(CH_3)NH]_3)_n$), which is sensitive to air and soluble in both toluene and tetrahydrafuran. Any increase in temperature beyond 85 ℃ during ammonolysis reaction resulted in degradation of the monomer, as was clearly observed in the form of change in color from colorless to light brown.

After flushing the furnace initially with argon, the as-synthesized polymer was taken in small quantities in an alumina crucible and thermolyzed at 1300 ℃ with a heating rate of 5 ℃/min and dwelling time varying from 0 to 10 h at intervals of 2 h in argon atmosphere, for transforming the polymeric precursor into a ceramic. All the samples were allowed to furnace cool to room temperature at the end of their respective heating cycles. The ceramic yield obtained was ~50% in all cases.

2.2 Characterization

The obtained ceramics were pulverized using agate mortar and pestle and characterized using XRD and Raman spectroscopy.

The X-ray diffractograms were obtained within the 2θ scan range of 10° to 90° with a step size of 0.05° using X'Pert PRO diffractometer, PANalytical (the Netherlands) with Cu Kα radiation of $\lambda = 0.154\,06$ nm, voltage of 45 kV and current of 30 mA. The background noise was subtracted after the removal of the $K\alpha_2$ peaks and the peak at $2\theta = 36°$ was chosen for crystal size measurement.

The Raman spectra of the as-thermolyzed ceramics were obtained in the scan range of 100 cm^{-1} to 3000 cm^{-1} from Labram HR800 UV-Raman Spectrometer equipped with charge coupled detector, Horiba Jobin Yvon (Japan) using a He–Ne laser source with an excitation wave length of $\lambda = 632.8$ nm. An Olympus BX-41 microscope with a 100× magnification was used to image the samples. The spectrometer was calibrated using silicon standard prior to Raman measurement.

3 Results and discussion

The X-ray diffractograms of the ceramic samples, thermolyzed at 1300 ℃ for various dwelling time, are shown in Fig 1. The hump at ~36° in the X-ray diffractogram of the ceramic sample thermolyzed at 1300 ℃ with no dwelling time (0 h) shows silicon carbide (SiC) as the first phase to nucleate from the amorphous Si–B–C–N quaternary ceramic. The nucleated crystals seem to grow with increase in dwelling time from 0 to 10 h, as can be seen in the predominant peaks in XRD of ceramic samples at 35.9°, 60.06° and 72.2°. The peaks are observed to be quite broad, thereby indicating the nano-crystalline nature of SiC. Cai *et al*. [20] has shown that nucleation of nano-crystallites in as-thermolyzed Si–B–C–N processed from boron-modified polysilazane, starts only at 1350 ℃ and remains completely amorphous below 1350 ℃. However, Gao *et al*. [33] has shown that the crystallization behavior of powder sample is quite different from that of bulk sample. The powder sample is found to crystallize at lower temperature and faster rate which is due to the sensitivity of the solid state of PDC to the molecular structure of the precursor. The peak at $2\theta = 36°$ was subjected to Pseudo-Voigt profile function fit to determine the full width at half

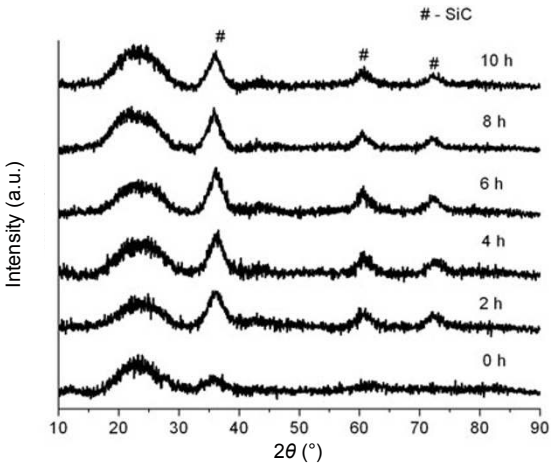

Fig. 1 X-ray diffractograms of the as-thermolyzed Si–B–C–N ceramic at 1300 ℃ for various dwelling time (heating rate of 5 ℃/min).

maximum (FWHM) and the crystallite diameter d was determined using the Scherrer formula (Eq. (1)):

$$d = \frac{K\lambda}{B\cos\theta} \quad (1)$$

where B is the FWHM; θ is the position of the peak; λ is the wavelength.

The crystallite size is found to be in the range of 2–8 nm and increases linearly with respect to dwelling time as shown in Fig. 2. The amorphous hump found from ~18° to ~28° in all the samples indicates the semi-crystalline nature of the ceramic. Hence, the percentage of crystallinity of the Si–B–C–N ceramic was calculated using Eq. (2):

$$\text{Crystallinty}(\%) = \frac{\sum I_{\text{peaks of SiC}}}{\sum I_{\text{all peaks}}} \quad (2)$$

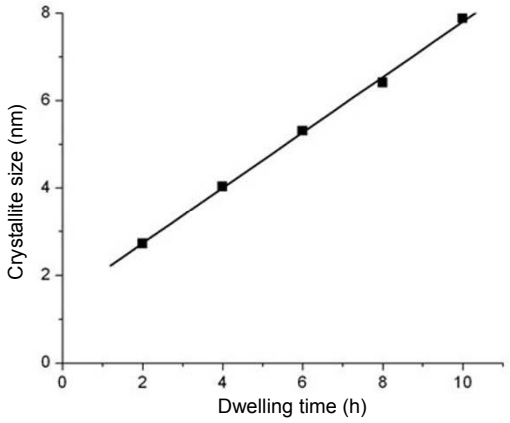

Fig. 2 Crystallite size of SiC of the as-thermolyzed Si–B–C–N ceramic at 1300 ℃ for various dwelling time (heating rate of 5 ℃/min) showing a linear fit.

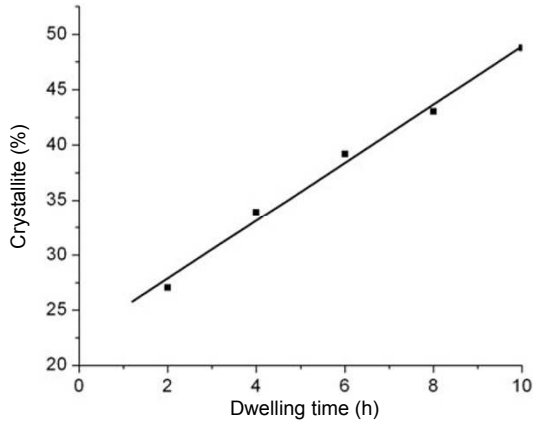

Fig. 3 Percentage of crystallinity in the as-thermolyzed Si–B–C–N ceramic at 1300 ℃ for various dwelling time (heating rate of 5 ℃/min) showing a linear fit.

The percentage of crystallinity is found to increase linearly with increase in dwelling time as shown in Fig. 3. The ceramic sample thermolyzed for 10 h is found to be ~50% crystallized, an increase when compared to ~25% crystallization found for the ceramic sample thermolyzed for 2 h. The increase in both crystal size and crystallinity of SiC indicate the occurrence of reaction between silicon and carbon present in the material, leading to the consumption of carbon. Hence, to determine the nature of the free carbon and its variation with crystallization, Raman spectroscopy was carried out.

Raman spectra of the as-thermolyzed Si–B–C–N ceramic at different dwelling time are shown in Fig. 4. The Raman spectra show two strong peaks at ~1325 cm^{-1} and ~1595 cm^{-1} for all samples, indicating the presence of free carbon. These two peaks are generally denoted as disordered peak (D peak) and graphitic peak (G peak), respectively. The G peak indicates the presence of graphite-like structure of carbon and corresponds to the in-plane bond stretching mode E_{2g} of the sp^2 C–C bond. This is found in pure graphite with no sp^3 hybridized carbon at 1575 cm^{-1} as a single peak, while in diamond with 100% sp^3 hybridized carbon, a single peak at 1332 cm^{-1} is found. Presence of sp^3 bonds (diamond-like arrangement) along with sp^2 bonds in carbon results in a second peak at 1355 cm^{-1} called as D peak along with the G peak at 1575 cm^{-1} [35]. This D peak is due to Raman scattering of the sp^3 hybridized form of carbon bonded to silicon present in the amorphous matrix. This D peak corresponds to the A_{1g} breathing mode of the aromatic ring. When structural disorder is present, the

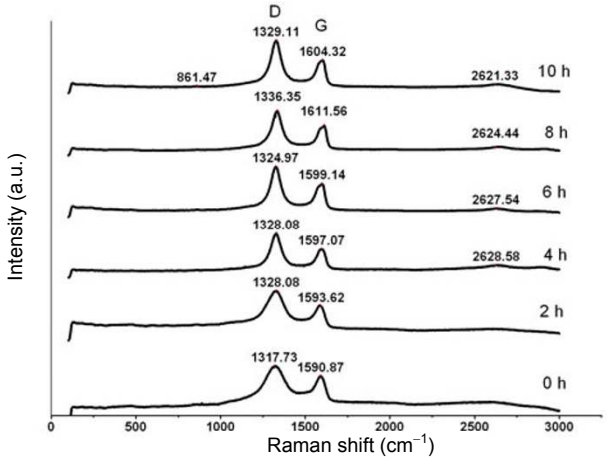

Fig. 4 Raman spectra of the as-thermolyzed Si–B–C–N ceramic at 1300 ℃ for various dwelling time (heating rate of 5 ℃/min).

D peak will shift towards the lower wave number from 1355 cm^{-1} with an increase in intensity and narrowing of the peak. The position of D peak is completely dependent on the excitation energy used which varies from ~1300 cm^{-1} to ~1400 cm^{-1} [36,37].

In general, sp^2 hybridized carbon has a tendency to cluster, and these clusters and their degree of clustering play crucial roles in determining the material properties [38–41]. This cluster diameter (L_a) is inversely proportional to the relative intensity of the D and G peaks and can be determined by the TK (Tuinstra and Koenl) equation [35]:

$$\frac{I_D}{I_G} = \frac{C(\lambda)}{L_a} \tag{3}$$

where I_D is the peak intensity of D band in Raman spectra; I_G is the peak intensity of G band in Raman spectra; and $C(\lambda)$ is the wavelength-dependent constant [42]:

$$C(\lambda) = C_0 + \lambda_L C_1 \tag{4}$$

where $C_0 = -12.6$ nm; $C_1 = 0.033$; λ_L is the wavelength used (632.8 nm).

Based on the aforementioned equation, L_a was calculated and observed to decrease from 6.2 nm to 5.4 nm as shown in Fig. 5 with increase in dwelling time. As the cluster diameter decreases, the sp^2 bond in carbon cluster tends to open, indicating the shift from sp^2 hybridization to sp^3 hybridization. This leads to transformation of graphite to nano-crystalline graphite, followed by amorphous carbon and finally forming tetrahedral amorphous carbon, also known as DLC (diamond-like carbon) which is termed *amorphization trajectory* in carbon materials [40,41].

With decrease in cluster size, the position of G peak shifts towards higher wave number, as shown in Fig. 6. The G band is observed to shift from 1590 cm^{-1} to 1611 cm^{-1} with increase in dwelling time from 0 to 8 h indicating the transformation of graphite to nano-crystalline graphite, resulting in disorder of the free carbon. A decrease in shift of G band towards 1600 cm^{-1} for sample thermolyzed at dwelling time of 10 h indicates the transformation of nano-crystalline graphite to amorphous carbon. This shows the increasing disorder in the structure of the free carbon with an increase in the contribution of sp^3 bond in the as-thermolyzed PDC. Unlike the D peak, the position of the G peak does not vary with the excitation energy used but is dependent on the cluster size [35]. The transformation of graphite to nano-crystalline graphite and finally to amorphous carbon indicates the opening up of the sp^2 carbon cluster, resulting in free sites which tend to react with the silicon present in the material, leading to the formation of SiC. This is clearly evident from the XRD data showing the increase in the crystallinity of SiC with increase in dwelling time.

From Fig. 5 it is clear that, the slope is steeper for dwelling time varying from 0 to 4 h, which indicates that the sp^2 hybridized bonds open up at a faster rate. However, for higher dwelling time (beyond 4 h), the relatively shallow slope indicates that the rate of opening up of bonds reduces considerably. Also, Fig. 2 shows that the crystal size of SiC is observed to increase linearly with increase in dwelling time, irrespective of the rate of opening up of sp^2 bonds. This is explained by the fact that at lower dwelling

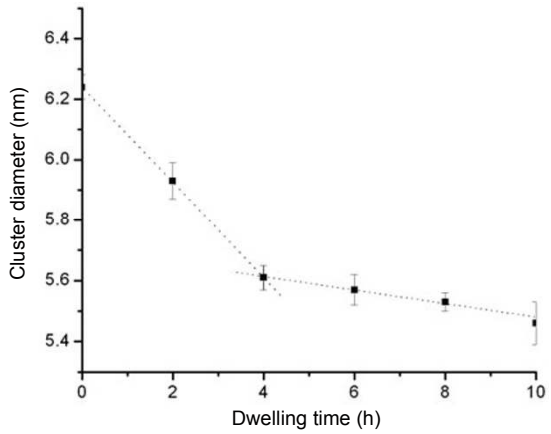

Fig. 5 Cluster size of carbon of the as-thermolyzed Si–B–C–N ceramic at 1300 ℃ for various dwelling time (heating rate of 5 ℃/min) showing change in rate of opening up of bonds in free carbon cluster at 4 h.

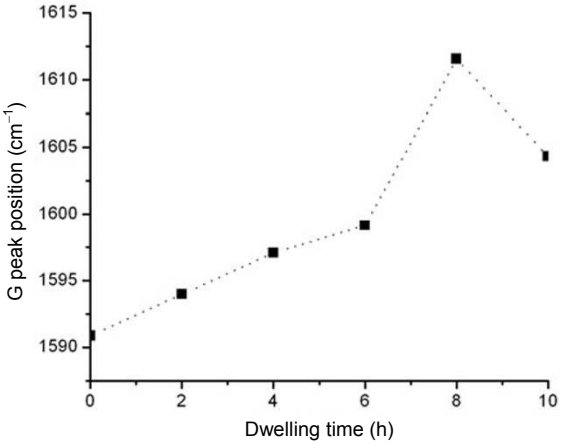

Fig. 6 Shift in the position of G peak for various dwelling time showing the transformation of graphite to nano-crystalline graphite and finally to amorphous carbon.

time (0–4 h), the predominant mechanism of nucleation of SiC crystal is the consumption of the free carbon, while for higher dwelling time varying from 6 h to 10 h, the growth is governed by Ostwald ripening. A low intensity peak can be observed at 861.47 cm^{-1} for the sample thermolyzed at 10 h, corresponding to SiC (Fig. 4). The low intensity is due to the fact that compared to the free carbon, optical absorption of SiC is lower by a factor of 10 [43]. Also, along with the D and G peaks, additional peak is obtained at ~2628 cm^{-1} for all samples and this corresponds to the presence of G′ band, better known as the second-order spectra of crystalline graphite [44].

The FWHM of D and G peaks are calculated by fitting the peaks using Lorentzian fit and the values are listed in Table 1. The FWHM values for both peaks are found to decrease with an increase in disorder of carbon present. In general, FWHM of G peak ($FWHM_G$) is directly related to the structural disorder present, since it arises due to the distortions in bond length and bond angle. Hence, it tends towards zero if clusters formed are defect-free and unstrained like pure graphite. But, on the contrary, a decrease in $FWHM_G$ is observed with an increase in disorder, whereas relative intensity (I_D/I_G ratio) increases as exemplified in Fig. 7, which is in accordance with the published literature on free carbon in polymer derived ceramics [30,45]. The decrease in $FWHM_G$ with increase in the position of G peak when graphene is doped with a secondary element that can act as electron or hole dopant as shown by Casiraghi *et al*. [46] further corroborates the aforementioned argument. Hence, the anomalous decrease in $FWHM_G$ with increase in structural disorder observed in the as-thermolyzed ceramic is possibly attributed to the presence of elements like silicon, nitrogen and boron, bonded to each other in various forms [47] within the free carbon phase.

Table 1 Peak positions, FWHM and intensities of D and G bands in the Raman spectra and ratio of their intensities and cluster diameter of carbon

Dwelling time (h)	Position of D peak (cm^{-1})	FWHM of D peak (cm^{-1})	Position of G peak (cm^{-1})	FWHM of G peak (cm^{-1})	I_D (a.u.)	I_G (a.u.)	I_D/I_G	L_a (nm)
0	1321.79	144.94	1590.87	77.08	11 142.39	8364.04	1.33	6.24
2	1324.00	116.90	1593.97	70.05	13 604.00	9684.71	1.40	5.93
4	1327.16	75.11	1597.07	67.22	6 187.14	4158.02	1.48	5.61
6	1325.89	73.09	1599.14	63.61	13 977.10	9368.38	1.49	5.57
8	1332.83	71.63	1611.56	55.29	12 241.79	8138.84	1.50	5.53
10	1327.40	70.81	1604.32	54.57	8 822.94	5776.20	1.52	5.46

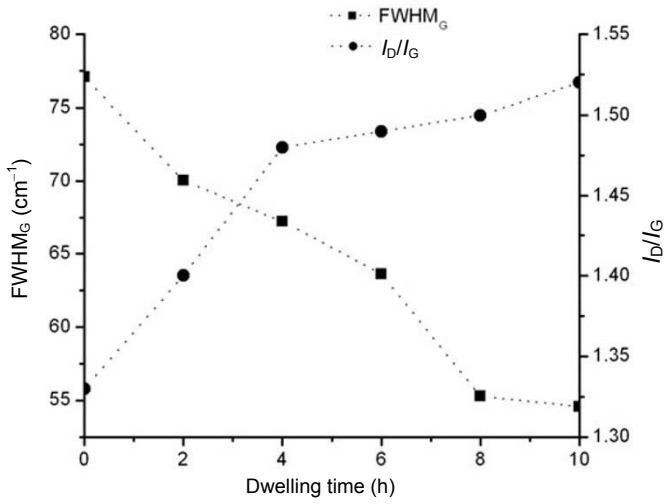

Fig. 7 Anomalous relation between $FWHM_G$ and I_D/I_G as functions of dwelling time.

4 Conclusions

Polyorganoborosilazane ($(B[C_2H_4–Si(CH_3)NH]_3)_n$) synthesized from a single-source precursor by monomer route was thermolyzed into Si–B–C–N ceramic and characterized to detect the presence of free carbon and formation of any crystalline phase. The presence of nano-crystalline SiC along with free carbon was observed in the as-thermolyzed ceramic. The cluster size of free carbon was calculated from Raman spectra and found to decrease with increase in dwelling time, thus indicating an increase in the extent of disorder in free carbon phase. XRD studies of the as-thermolyzed Si–B–C–N ceramic revealed nucleation of SiC crystal as the first phase along with increase in crystal size and crystallinity with increase in dwelling time. In this work, the role of free carbon

on the crystallization behavior, the bonding character of the free carbon present and the change in the ratio of sp^2 hybridization to sp^3 hybridization of free carbon were studied.

Acknowledgements

We gratefully acknowledge the financial support from the Vikram Sarabhai Space Centre, Thiruvananthapuram through ISRO-IITM cell (Project No. ICSR/ISRO-IITM/MET/08-09/122/RAVK). We also would like to acknowledge the Department of Physics, IIT-M for performing Raman spectroscopy.

References

[1] Houtz RC. "Orlon" acrylic fiber: Chemistry and properties. *Text Res J* 1950, **20**: 786–801.

[2] Ezekiel HM, Spain RG. Preparation of graphite fibers from polymeric fibers. *J Polym Sci Pol Sym* 1967, **19**: 249–265.

[3] Verbeek W. Production of shaped articles of homogeneous mixtures of silicon carbide and nitride. U.S. Patent 3853567 A, Nov. 1973.

[4] Verbeek W, Winter G. Formkoerper aus siliciumcarbid und verfahren zu ihrer herstellung. DE Patent 2236078 A1, July 1974.

[5] Yajima S, Hayashi J, Imori M. Continuous silicon carbide fiber of high tensile strength. *Chem Lett* 1975, **4**: 931–934.

[6] Hayashi J, Omori M, Yajima S. Siliciumcarbidfasern und verfahren zur herstellung derselben. DE Patent 2618150 A1, April 1976.

[7] Yajima S, Hayashi J, Omori M, *et al*. Development of a silicon carbide fiber with high tensile strength. *Nature* 1976, **261**: 683–685.

[8] Bernard S, Weinmann M, Cornu D, *et al*. Preparation of high-temperature stable Si–B–C–N fibers from tailored single source polyborosilazanes. *J Eur Ceram Soc* 2005, **25**: 251–256.

[9] Bernard S, Weinmann M, Gerstel P, *et al*. Boron-modified polysilazane as a novel single-source precursor for SiBCN ceramic fibers: Synthesis, melt-spinning, curing and ceramic conversion. *J Mater Chem* 2005, **15**: 289–299.

[10] Miele P, Bernard S, Cornu D, *et al*. Recent developments in polymer-derived ceramic fibers (PDCfs): Preparation, properties and applications—A review. *Soft Mater* 2007, **4**: 249–286.

[11] Sarkar S, Zhai L. Polymer-derived non-oxide ceramic fibers—Past, present and future. *Mater Express* 2011, **1**: 18–29.

[12] Mucalo MR, Milestone NB, Vickridge IC, *et al*. Preparation of ceramic coatings from pre-ceramic precursors. *J Mater Sci* 1994, **29**: 4487–4499.

[13] Hauser R, Borchard SN, Riedel R, *et al*. Polymer-derived SiBCN ceramic and their potential application for high temperature membranes. *J Ceram Soc Jpn* 2006, **114**: 524–528.

[14] Torrey JD, Bordia RK. Processing of polymer-derived ceramic composite coatings on steel. *J Am Ceram Soc* 2008, **91**: 41–45.

[15] Schütz A, Günthner M, Motz G, *et al*. Characterisation of novel precursor-derived ceramic coatings with glass filler particles on steel substrates. *Surf Coat Technol* 2012, **207**: 319–327.

[16] Riedel R, Kienzle A, Dressler W, *et al*. A silicoboron carbonitride ceramic stable to 2,000 ℃. *Nature* 1996, **382**: 796–798.

[17] Müller A, Gerstel P, Weinmann M, *et al*. Correlation of boron content and high temperature stability in Si–B–C–N ceramics. *J Eur Ceram Soc* 2000, **20**: 2655–2659.

[18] Müller A, Gerstel P, Weinmann M, *et al*. Correlation of boron content and high temperature stability in Si–B–C–N ceramics II. *J Eur Ceram Soc* 2001, **21**: 2171–2177.

[19] Wang Z-C, Aldinger F, Riedel R. Novel silicon–boron–carbon–nitrogen materials thermally stable up to 2200 ℃. *J Am Ceram Soc* 2001, **84**: 2179–2183.

[20] Cai Y, Zimmermann A, Prinz S, *et al*. Nucleation phenomena of nano-crystallites in as-pyrolysed Si–B–C–N ceramics. *Scripta Mater* 2001, **45**: 1301–1306.

[21] Butchereit E, Nickel KG, Müller A. Precursor-derived Si–B–C–N ceramics: Oxidation kinetics. *J Am Ceram Soc* 2001, **84**: 2184–2188.

[22] Ramakrishnan PA, Wang YT, Balzar D, *et al*. Silicoboron–carbonitride ceramics: A class of high-temperature, dopable electronic materials. *Appl Phys Lett* 2001, **78**: 3076.

[23] Ravi Kumar NV, Mager R, Cai Y, *et al*. High temperature deformation behavior of crystallized Si–B–C–N ceramics obtained from a boron modified poly(vinyl)silazane polymeric precursor. *Scripta Mater* 2004, **51**: 65–69.

[24] Saha A, Raj R, Williamson DL. A model for the nanodomains in polymer-derived SiCO. *J Am Ceram*

Soc 2006, **89**: 2188–2195.

[25] Kumar R, Mager R, Phillipp F, *et al*. High-temperature deformation behavior of nanocrystalline precursor-derived Si–B–C–N ceramics in controlled atmosphere. *Int J Mater Res* 2006, **97**: 626–631.

[26] Colombo P, Mera G, Riedel R, *et al*. Polymer-derived ceramics: 40 years of research and innovation in advanced ceramics. *J Am Ceram Soc* 2010, **93**: 1805–1837.

[27] Hermann AM, Wang Y-T, Ramakrishnan PA, *et al*. Structure and electronic transport properties of Si–(B)–C–N ceramics. *J Am Ceram Soc* 2001, **84**: 2260–2264.

[28] Wang Y, Wang K, Zhang L, *et al*. Structure and optical property of polymer-derived amorphous silicon oxycarbides obtained at different temperatures. *J Am Ceram Soc* 2011, **94**: 3359–3363.

[29] Peng J. Thermochemistry and constitution of precursor-derived Si–(B–)C–N ceramics. Ph.D. Thesis. Stuttgart (Germany): Universität Stuttgart, 2002.

[30] Trassl S, Motz G, Rössler E, *et al*. Characterization of the free-carbon phase in precursor-derived SiCN ceramics: I, spectroscopic methods. *J Am Ceram Soc* 2002, **85**: 239–244.

[31] Mera G, Riedel R, Poli F, *et al*. Carbon-rich SiCN ceramics derived from phenyl-containing poly(silylcarbodiimides). *J Eur Ceram Soc* 2009, **29**: 2873–2883.

[32] Sarkar S, Gan Z, An L, *et al*. Structural evolution of polymer-derived amorphous SiBCN ceramics at high temperature. *J Phys Chem C* 2011, **115**: 24993–25000.

[33] Gao Y, Mera G, Nguyen H, *et al*. Processing route dramatically influencing the nanostructure of carbon-rich SiCN And SiBCN polymer derived ceramics. Part I: Low temperature thermal transformation. *J Eur Ceram Soc* 2012, **32**: 1857–1866.

[34] Kumar R, Cai Y, Gerstel P, *et al*. Processing, crystallization and characterization of polymer derived nano-crystalline Si–B–C–N ceramics. *J Mater Sci* 2006, **41**: 7088–7095.

[35] Tunistra F, Koenig JL. Raman spectrum of graphite. *J Chem Phys* 1970, **53**: 1126–1130.

[36] Pócsik I, Hundhausen M, Koós M, *et al*. Origin of the D peak in the Raman spectrum of microcrystalline graphite. *J Non-Cryst Solids* 1998, **227–230**: 1083–1086.

[37] Ferrari AC. Raman spectroscopy of graphene and graphite: Disorder, electron–phonon coupling, doping and nonadiabatic effects. *Solid State Commun* 2007, **143**: 47–57.

[38] Jiang T, Wang Y, Wang Y, *et al*. Quantitative Raman analysis of free carbon in polymer-derived ceramics. *J Am Ceram Soc* 2009, **92**: 2455–2458.

[39] Robertson J. Hard amorphous (diamond-like) carbons. *Prog Solid State Ch* 1991, **21**: 199–333.

[40] Ferrari AC, Robertson J. Interpretation of Raman spectra of disordered and amorphous carbon. *Phys Rev B* 2000, **61**: 14095–14107.

[41] Ferrari AC, Robertson J. Raman spectroscopy of amorphous, nanostructured, diamond-like carbon, and nanodiamond. *Phil Trans R Soc Lond A* 2004, **362**: 2477–2512.

[42] Matthews MJ, Pimenta MA, Dresselhaus G, *et al*. Origin of dispersive effects of the Raman *D* band in carbon materials. *Phys Rev B* 1999, **59**: R6585–R6588.

[43] Ma Y, Wang S, Chen Z. Raman spectroscopy studies of the high-temperature evolution of the free carbon phase in polycarbosilane derived SiC ceramics. *Ceram Int* 2010, **36**: 2455–2459.

[44] Pimenta MA, Dresselhaus G, Dresselhaus MS, *et al*. Studying disorder in graphite-based systems by Raman spectroscopy. *Phys Chem Chem Phys* 2007, **9**: 1276–1290.

[45] Trassl S, Motz G, Rössler E, *et al*. Characterisation of the free-carbon phase in precursor-derived SiCN ceramics. *J Non-Cryst Solids* 2001, **293–295**: 261–267.

[46] Casiraghi C, Pisana S, Novoselov KS, *et al*. Raman fingerprint of charged impurities in grapheme. *Appl Phys Lett* 2007, **91**: 233108.

[47] Ravi Kumar NV, Prinz S, Cai Y, *et al*. Crystallization and creep behavior of Si–B–C–N ceramics. *Acta Mater* 2005, **53**: 4567–4578.